Real-time, *in situ* film thickness metrology in a 10 Torr W chemical vapor deposition process using an acoustic sensor

L. Henn-Lecordier, J. N. Kidder, Jr., and G. W. Rubloff[a)]
Department of Materials and Nuclear Engineering and Institute for Systems Research, University of Maryland, College Park, Maryland 20742

C. A. Gogol and A. Wajid
Inficon, Inc., East Syracuse, New York 13057

(Received 24 June 2002; accepted 10 February 2003; published 5 May 2003)

Process gases were sampled from the outlet of a tungsten chemical vapor deposition (CVD) reactor into an Inficon Composer™ acoustic sensor for *in situ* chemical gas sensing and real-time film thickness metrology. Processes were carried out on an Ulvac W CVD cluster tool at 10 Torr from 340 to 400 °C using a H_2/WF_6 gas mixture. Sampled gases were compressed through a diaphragm pump up to 100 Torr as required for accurate measurements in the acoustic cell. The high depletion of the heavy WF_6 precursor (up to 30%) generated a significant variation of the average gas molecular weight and consequently of the mass-dependent resonant frequency measured by the acoustic sensor. The monitored signal was integrated over the process time, and the integrated area was correlated to the deposited W film thickness determined by *ex situ* measurements. The average error on this in-tool and real-time metrology was less than 1% over 30 wafers processed, either under fixed process conditions or while varying key process variables such as deposition time or temperature. A dynamic physically based simulator was also developed to validate the system response under different process conditions and demonstrate the fundamental understanding of this method. The metrology achieved represents a significant improvement over previously published data [L. Henn-Lecordier *et al.*, J. Vac. Sci. Technol. A **19**, 621 (2001)] obtained on the same system but in the sub-Torr process pressure regime, where low depletion rates (around 3%) had limited the metrology to 7% error. With an error less than 1%, this *in situ* chemical sensing approach could be efficiently exploited for real-time course correction, e.g., using end-point film thickness control. [DOI: 10.1116/1.1565342]

I. INTRODUCTION

The implementation of Advanced Process Control (APC) methodologies in semiconductor manufacturing is becoming a key productivity asset in 300 mm fabs by minimizing equipment down time and test wafer consumption.[1,2] The International Technology Roadmap for Semiconductors[3] places an emphasis on two APC components, both fault management and process course correction. To date, the primary implementations of APC have been in real-time fault detection to detect equipment failures, and on run-to-run process control to reduce process variability, especially in the areas of chemical-mechanical polishing and lithography processing. For the most part, real-time course correction has yet to emerge as a significant component of a comprehensive real-time APC strategy.

Little has been reported in manufacturing to implement real-time film thickness control in chemical vapor deposition (CVD) processes, even though this could significantly reduce production costs by reducing the number of qualification wafers required for process stability. If real-time process metrology and control could be achieved, it would enable tighter film thickness control in the presence of random disturbances as well as systematic long-term process drifts, whereas run-to-run control is effective only for the latter. However, real-time end-point film thickness control in CVD is challenging because adequate methodology for *in situ* metrology is not yet available. Not only must the in-tool and real-time sensor-based metrology yield reproducible results with an error less than 1% or so, but it must be achieved with a minimal impact on the process (e.g., cycle time or chemical contamination) while ensuring that sensor robustness and reliability are not limiting factors.

Different *in situ* approaches have been reported for film thickness metrology, from direct thickness measurement techniques that look directly at the surface of the wafer[4,5] to indirect measurements using *in situ* or downstream gas sensing methods. Gas phase measurements in CVD processes were reported using ultraviolet,[6–8] Fourier-transform infrared (FTIR)[9–14] and mass spectrometry.[15–20] Our group recently reported achieving film thickness metrology with a 2% error using mass spectrometry (or residual gas analysis) in blanket W CVD processes with WF_6 and highly reactive SiH_4 in the sub-Torr pressure regime, sufficient to demonstrate both run-to-run and real-time end-point control within a 1%–3% accuracy from the selected thickness target.[21,22] In parallel with this research based on mass-spectrometry sensing of specific chemical species, we have been investigating the utilization of a technically simpler sensor, an acoustic sensor which monitors total gas composition as reflected in its average molecular weight. Specifically, we have been using the Infi-

a)Electronic mail: rubloff@isr.umd.edu

con Composer™, which was originally designed and commercialized for upstream composition measurements and control of binary gas mixtures in metalorganic (CVD) systems using a temperature and pressure-controlled ''bubbler'' source in order to enhance the process.[23–28] Its potential use for in-situ calibration of mass flow controllers was also reported.[29]

The Inficon acoustic sensor measures in a thermally controlled acoustic cavity the resonant frequency of a gas mixture, which is directly related to its average molecular weight[30] as shown in Eq. (1):

$$F = \frac{c}{2L} \quad \text{with} \quad c = \sqrt{\frac{\gamma_{\text{avg}} RT}{M_{\text{avg}}}}, \tag{1}$$

where F=gas resonant frequency; c=sound velocity; γ_{avg}=average specific heat ratio; T=gas temperature; M_{avg}=average molecular weight; R=gas constant; and L=length of acoustic cell.

Because of the high sensitivity of acoustic sensors when measuring even minute concentrations of high molecular weight precursors in a low molecular weight carrier gas such as H_2, it was expected that this sensor could be implemented downstream to a W CVD process chamber in order to monitor the depletion of heavy WF_6 precursor mixed with H_2 when depositing a tungsten film.

Previously, we reported promising preliminary results in a W CVD process at 0.5 Torr using a H_2/WF_6 gas mixture.[31] *In situ* film thickness metrology was established with an average 6% error which was at the time similar to other results obtained by mass-spectrometry measurements carried out for the same process.[19] Both the acoustic and mass spectrometry based metrologies were seriously limited in accuracy by the low conversion rate of the reactants (~3%) achieved with the low pressure (sub-Torr) operation of the Ulvac reactor. Our preliminary conclusion was that the acoustic sensor sensitivity was not the limiting factor and that higher depletion rates of 30% or more, which is common in manufacturing blanket W CVD, would significantly improve the signal to noise ratio and lead to a significant improvement of the metrology, making it suitable for APC applications. Another drawback was that prior to each deposition a baseline measurement, with WF_6 and H_2 flowing in the chamber at room temperature, was needed. That base line data had to be subtracted from the signal obtained during deposition in order to correct for a systematic process drift due primarily to wall reactions whose effect was non-negligible compared to the variation of the average molecular weight caused by the low precursor depletion. This extra step resulted in a significant increase of the process cycle time, making this approach non suitable for manufacturing.

In order to demonstrate improved performance of thickness metrology based on acoustic sensing under more realistic manufacturing process conditions (i.e., higher pressures), significant modifications of the process tool and sampling system were therefore undertaken. This article will discuss these changes and their impact by presenting three main sets of data, some obtained under fixed process conditions at 390 °C and 10 Torr, and the others acquired while varying key process metrics such as temperature and process times.

In addition, a system level simulation of the process tool and sampling system was developed. The sensor output [Eq. (1)] as a function of the gas composition was integrated over time in the simulation to evaluate the system response under various process conditions and to validate the assumptions on which this acoustic sensing method is based. This complements our earlier work, in which the basic assumptions (e.g., sensor response as a function of flow rates and partial pressures) had been explored through simulation, but only under steady state conditions and without product generation or reactant depletion.

II. EXPERIMENT

Experiments were carried out on a production scale Ulvac ERA 1000 W CVD cluster tool which is outfitted with water-cooled walls. The WF_6 precursor was introduced from a side slot located at wafer height while H_2 was inlet from a circular quartz showerhead located 5 in. above the wafer. The process gases were pumped away by a Roots blower pump backed up with a mechanical rotary pump, while a turbomolecular pump was used to maintain cleanliness in idle mode. The process pressure was measured with a capacitance diaphragm gauge coupled to a downstream low-conductance throttle valve, and gas flows were regulated through mass flow controllers. To allow processing at pressure above 1 Torr, the wafer heating mechanism was converted from lamp heating through a window to direct heating by a resistive substrate heater. Temperatures reported in this article are actual wafer temperatures as determined by an instrumented wafer with thermocouple sensors. Si wafers (4 in. diam) were dipped in 10% HF solution for 20 min to remove the native oxide, rinsed with de-ionized water, blown dry with nitrogen, and transferred within a few minutes into the CVD reactor through a high vacuum load-lock chamber.

Processes were carried out at 10 Torr using a H_2/WF_6 gas mixture with a 6/1 flow ratio. Typically the processing of a wafer batch was carried out as follows: the reactor walls were initially conditioned for 1–2 h (determined by the chamber process history) by flowing WF_6 and H_2 at 10 Torr at room temperature in order to reduce the amount of water in the chamber and to passivate the walls. Of course, such chamber wall conditioning process would be unrealistic for manufacturing, though it was needed to stabilize the operating conditions of our reactor. It is important to recognize, however, that the high wafer throughput used on a manufacturing tool would be much more effective in achieving steady-state conditions of the chamber walls than we have achieved here. Accordingly, there should be no need for any extra conditioning step in manufacturing. For that matter, we expect that the high throughput seen by tools in manufacturing may well result in improved sensor-based metrology than we are able to achieve in a research environment.

The H_2O partial pressure as well as WF_6/WOF_4 ratio were monitored using a 300 amu closed ion source mass spectrometer mounted on the chamber. After conditioning,

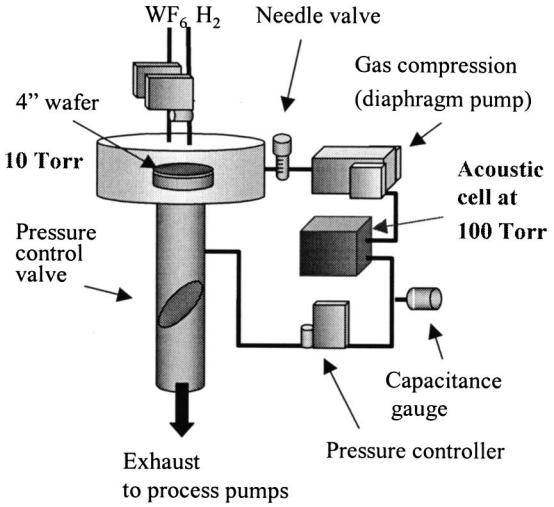

FIG. 1. CVD reactor and sampling system. Process gases are sampled from the 10 Torr CVD reactor into the acoustic transducer. A diaphragm pump is used to compress the process gases from 10 to 100 Torr to insure a sufficient gas media density for accurate acoustic wave measurements.

the chamber was purged with N_2 and the heater temperature was ramped over 30 min to the desired process temperature to insure stable temperature conditions. The first wafer was then directly transferred from the load-lock onto the hot substrate heater. After a 2 min delay to stabilize the temperature, the process was initiated. Typical processes recipes included three steps: (1) The H_2/WF_6 gas mixture was inlet with 600 sccm H_2 and 100 sccm WF_6 for 18 s. The high flows were required to ramp the process pressure in the 25 L chamber up to 10 Torr in a reasonably short time. (2) Once at 10 Torr, H_2 and WF_6 gas flows were respectively reduced to 60 and 10 sccm to minimize the reactant usage, which in turn enhances metrology signals associated with reactant depletion and product generation. The deposition times studied varied from 3 to 15 min. (3) At completion of the deposition step, the chamber was pumped down and then purged with N_2 for 600 s. Though this purge was not required by the process, it was useful for detecting any potential long term or run-to-run sensitivity variations in the sensor. The processed wafer was then unloaded and a new one introduced.

The sampling system for the acoustic sensor is shown in Fig. 1. Process gases were sampled a few inches downstream from the wafer through a 1/4 in. stainless steel tubing. To ensure a sufficient gas density in the acoustic cell for acoustic wave propagation (i.e., total pressure >50 Torr), a 0.5 CFM leak-tight Pfeiffer MVP 015 diaphragm pump was implemented upstream to the sensor (i.e., between reactor and acoustic sensor) to compress the process gases. A capacitance pressure gauge was coupled with a solenoid proportional valve downstream to the sensor in order to control the pressure at 100 ± 1 Torr in the acoustic cell. The total gas flow was estimated from a N_2 calibrated mass flow meter. The sampling line and the acoustic cavity were temperature controlled at 60 °C to limit the condensation of WF_6.

The gas throughput through the cell was initially adjusted with a metering valve upstream to the pump. Using N_2, the conductance of the metering valve was set so that the steady state flow was 10 sccm with a 10 Torr inlet pressure. This insured a residence time of 35 s in the sampling system, which was at a pressure of 100 Torr and had an estimated volume of 45 cm^3. The residence time in the sampling system was approximately an order of magnitude less than the residence time in the 25 l reactor at 10 Torr during the process.

The synthesized stimulating frequency was varied by a lock-in amplifier integrated in the Inficon sensor controller in order to remain in resonance with the gas flowing through the cell with a 1 s time resolution. The time-stamped data were saved to a text file for postprocessing.

After each run, the amount of W deposited was determined by an *ex situ* film weight measurement using a microbalance with a 1^{-4} g resolution. The average film thickness was then estimated based on the weight of deposited tungsten and its bulk density. Typical film weight and thickness were therefore estimated at approximately $\pm0.1\%$ based on a high estimate $(5\times10^{-4}\,\mathrm{g})$ of the weight error.

III. DYNAMIC SIMULATION

Based on previously published work,[32] a physically based simulation was developed to assess the time-dependent variations of the partial pressures in the chamber during the process, and correspondingly to determine the expected resonant frequency of the acoustic sensor under various gas flow conditions in the chamber. A Windows-based simulation engine, VisSim™ (Visual Solutions Inc.), was used for this continuous-parameter, nonlinear dynamic simulation. The gas flow calculation is based on the mass balance in the reactor, assuming ideal gas mixing. As shown in Eq. (2), instantaneous pressure in the chamber is determined by time integration of the net flux of molecules in/out of the chamber, taking into account reactant gas inlet, reactant gas depletion due to the reaction, generation of reaction products, and pumping of all gases out of the chamber

$$P = P_0 + \frac{1}{V}\int (Q_{\mathrm{in}} - Q_{\mathrm{out}} + Q_{\mathrm{reaction\_products}} - Q_{\mathrm{reactant\_depletion}})\,dt, \tag{2}$$

where P (Torr) = pressure in the chamber at time t; V (l) = chamber volume; P_0 (Torr) = initial pressure of the reaction chamber; Q_{in} (Torr l/s) = total gas throughput entering the reactor; Q_{out} (Torr l/s) = total gas throughput leaving the reactor; $Q_{\mathrm{reaction\_products}}$ (Torr l/s) = gas throughput created by product generation; and $Q_{\mathrm{reactant\_depletion}}$ (Torr l/s) = gas throughput lost from reactor due to reactant depletion.

The total gas throughput entering the reactor Q_{in} is established from the mass flow controller set points while $Q_{\mathrm{reaction\_products}}$ and $Q_{\mathrm{reactant\_depletion}}$ are determined from the WF_6 depletion rate during the reaction and the corresponding mole fractions of the other gases based on the stoichiometric equation for the W CVD reaction by H_2 reduction [Eq. (3)]. The WF_6 depletion rate was estimated experimentally from the weight of W deposited on the wafer

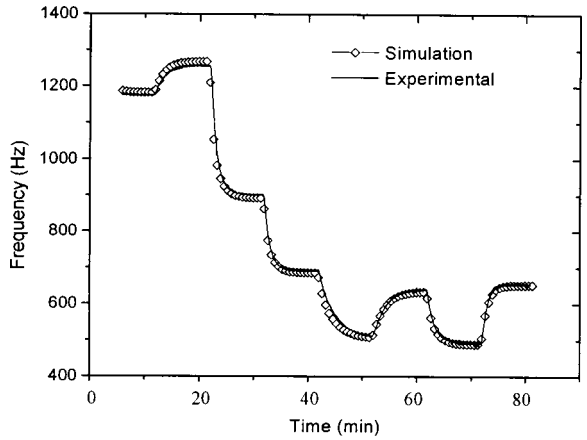

FIG. 2. Validation of dynamic simulation results. Simulation data show a good fit to experimental measurements of the resonant frequency for different gas compositions of WF_6:H_2:Ar flow into the reactor at room temperature (i.e., no reactant depletion or product generation).

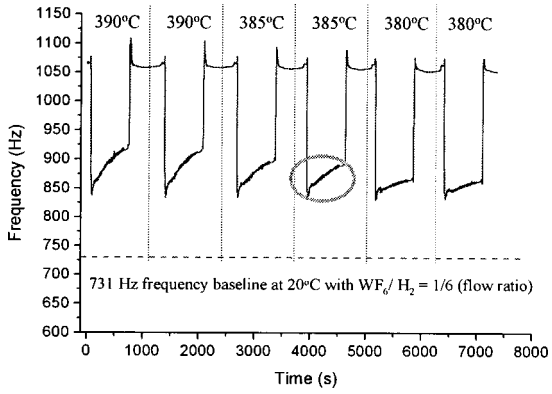

FIG. 3. Variation of the resonant frequency as a function of the time during six consecutive W CVD runs for temperatures varying from 390 to 380 °C. The steps at 1065 Hz correspond to the N_2 purge of the reactor in between runs. The lower depletion of WF_6 (shown in the contoured area) as the temperature goes down produces a decrease of the resonant frequency due to an increase of the average gas molecular weight.

$$WF_6\ (\text{gas}) + 3H_2\ (\text{gas}) \Rightarrow W\ (\text{solid}) + 6HF\ (\text{gas}). \quad (3)$$

Q_{out} represents the total gas throughput to the process pump and the sampling system. The effective gas throughput to the process pumps was estimated respectively for the Roots blower and the rotary backing pump based on Eq. (4). In this case, the pumping speed and compression ratio of the Roots blower and the rotary mechanical pump were assumed constant and established from the pump manufacturer's specifications

$$Q_{\text{eff}} = [(P_{\text{inlet}} - P_{\text{base}}) - (P_{\text{outlet}} - P_{\text{inlet}})/\text{CR}] \times \text{PS}, \quad (4)$$

where Q_{eff} (Torr l/s) = effective throughput through process pump; P_{inlet} (Torr) = pump inlet pressure; P_{base} (Torr) = pump base pressure; P_{outlet} (Torr) = pump outlet pressure; CR = pump compression ratio; and PS [l/s] = pumping speed.

The partial pressures for the reactants and reaction products were calculated from the product of the total pressure in the reactor [Eq. (2)] by the mole fraction of the chemical species estimated from the input gas flows and the WF_6 depletion rate. The average molecular weight and average specific heat ratio of the corresponding gas mixture were then computed to determine the resonant frequency of the acoustic sensor, based on Eq. (1). It should be noted that the resonant frequency is computed from the partial pressure of the chemical species in the reactor, as opposed to that in the acoustic cell. However, since the response time (or residence time) in the reactor is $>10\times$ larger than that in the sampling system, the simulation results are not significantly affected by this approximation.

To validate this simulation, a gas mixture of H_2, WF_6, and Ar was inlet with different flow rates varying from 0 to 200 sccm for 10 min time steps at room temperature (e.g., with no product generation or reactant depletion) with 10 Torr total pressure in the reactor.

Figure 2 shows the good fit between the experimental and simulation data of the mass dependent resonant frequency of the acoustic sensor. The time dependence in the simulation reflects accurately the intrinsic dynamics of the sensor and system response under different gas throughputs. The calculated resonant frequency varies as expected, with an offset between the simulation and the experimental data that likely results from some inaccuracies in the gas flow rates delivered by the mass flow controllers (MFCs) (especially for the H_2 MFC that is used only at 6% of the MFC full scale of 1000 sccm).

IV. RESULTS

A. Frequency measurements during one run

Figure 3 shows the variation of the acoustic sensor resonant frequency that was monitored continuously over time during the process of a batch of multiple wafers at different temperatures, where in this case six consecutive runs are shown. The steps at 1065 Hz corresponded to the N_2 purge in between processes.

Figure 4 shows in more detail the sensor response over

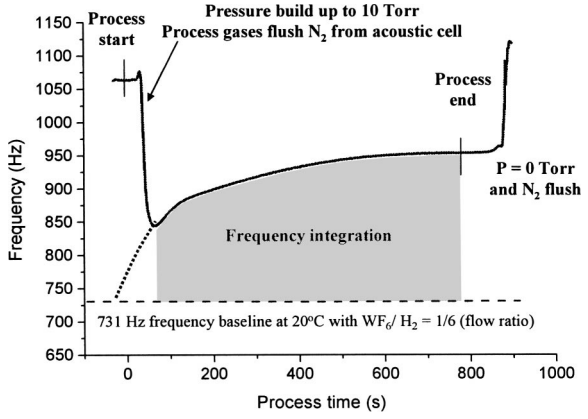

FIG. 4. Resonant frequency vs process time over one W CVD run. The film thickness metrology is established from the frequency integration whose limits are represented by the shaded area. The integration starts when the composition in the sensor images the composition in the reactor. The base line at 731 Hz corresponds to the frequency that would have been measured if no deposition was taking place on the wafer.

one run. Prior to the start of the deposition step, the acoustic cell was filled with N_2 at 100 Torr from the purge at the end of the previous run: since the pressure in the acoustic sensor was controlled by a downstream solenoid valve, the N_2 was contained in the sampling system when the purge of the process chamber was stopped and the pressure control valve on the sampling system closed. As the process started, H_2 and WF_6 were flowed into the process chamber and the pressure in the reactor built up from 0 to 10 Torr. The throughput of gases through the sampling system's mechanical pump increased with the pressure in the reactor and the N_2 in the sensor was replaced by the process gas mixture, resulting in a sharp drop of the resonant frequency. If no reaction was taking place, the frequency decreased down to 731 Hz, which corresponds to the resonant frequency for a binary gas mixture of H_2 and WF_6 with a 6 to 1 ratio at room temperature. When the wafer was heated and a reaction took place, WF_6 (with a high molecular weight, 276 g/mol) was depleted, W was deposited on the wafer, and the HF gas byproduct (20 g/mol) was generated. Consequently, the average molecular weight decreased, resulting in a resonant frequency higher than the 731 Hz value [see Eq. (1)]. At the end of the deposition step, the flow of reagents was stopped and the chamber was pumped down to 10^{-2} Torr in a few seconds. The sampling system pressure control valve therefore closed rapidly to maintain the pressure in the cell and the process gases remained in the cell. When the pressure in the chamber increased later on during the N_2 purge, the process gases were flushed from the cell and the frequency increased.

The deviation in frequency from 731 Hz to the actual frequency is caused by the extent of the precursor consumption. Therefore, the integration of the sensor signal from the time where the sensor is effectively sensing the composition changes in the reactor until the end of the process is a function of the amount of WF_6 consumed and the amount of W deposited in the reactor. Because the gas phase acoustic measurements reflect the overall gas composition in the chamber, the change in the resonant frequency might result not only from the amount of W deposited on the wafer but also on other surfaces of the reactor (see Sec. V).

B. Experiments at fixed process conditions

In the first set of experiments, a batch of ten wafers were processed under the same process conditions at 400 °C and 10 Torr for a fixed deposition time of 640 s. Figure 5 shows the correlation between the integration of the frequency over the deposition time and the deposited W film weight as measured by *ex situ* measurement on the left axis (the individual data points) and the estimated average film thickness on the right (the linear model). Because of the narrow distribution of the average film thickness over this batch (1609 nm±2%), the graph is shown with the *y* axis offset from zero.

The difference between the weight measurements and the corresponding values obtained from the computed linear fit were calculated for each point and averaged over the ten runs in order to provide a metric for the error of the *in situ* film thickness metrology. The average error for this batch according to this method was estimated to 0.5%.

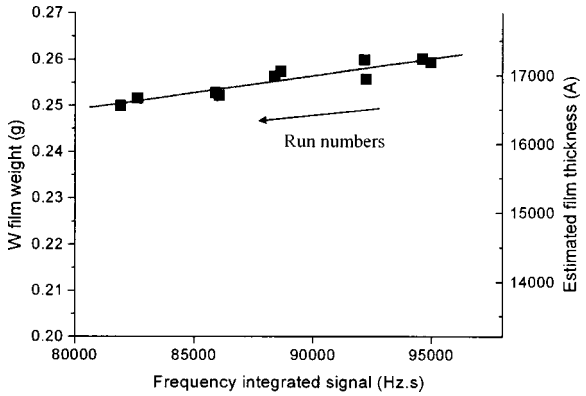

FIG. 5. Correlation between the integrated measurement of the sensor-based frequency and the deposited W film weight determined by *ex situ* measurements. A batch of ten wafers was processed at 400 °C and 10 Torr for 640 s. A 0.5% average metrology error was calculated based on the shown linear fit. It is similar to the observed 0.4% process drift per run of the deposited W film weight.

Despite the fixed process conditions, a systematic drift was observed over ten runs, with the deposited film weight decreasing by an average 0.4% per run. Run-to-run process drifts are not unusual in CVD tools; for example, WF_6 as used in W CVD reacts strongly with water vapor, and it is easily adsorbed on the walls or surfaces inside the reactor and delivery system. In our case, the run-to-run decrease of the W film thickness on the wafer is primarily attributed to the presence of an uncooled 80 $in.^2$ quartz showerhead located above the substrate heater (used previously with the lamp heating configuration). As its temperature increases over a period of several hours, W nucleation occurs on the showerhead, followed by increasing deposition on its surface. This effect is clearly visible by looking at the increasing opacity of the showerhead from run-to-run, as well as by the increase of the window temperature located on top of the showerhead.

C. Effect of run-to-run temperature drift

To understand the effects of a potential equipment drift on the process and the sensor based metrology, a batch of 18 wafers was processed for a fixed deposition time of 618 s. while varying the wafer temperature. The temperature was first decreased every two wafers by 5 °C from 400 to 380 °C, then by 10 °C down to 340 °C over the remaining eight wafers.

Figure 6 shows the variation of the resonant frequency as a function of the process time at five different temperatures. The effect of the temperature on the monitored signal is clearly visible. As the depletion rate of WF_6 decreases from one wafer to the next and the average gas molecular weight increases when the process temperature is lowered, the monitored frequency accordingly decreases. As in Fig. 5, the deposited W film weight and the estimated film thickness are displayed in Fig. 7 as a function of the frequency signal integrated over the process time. In this case it appears that a

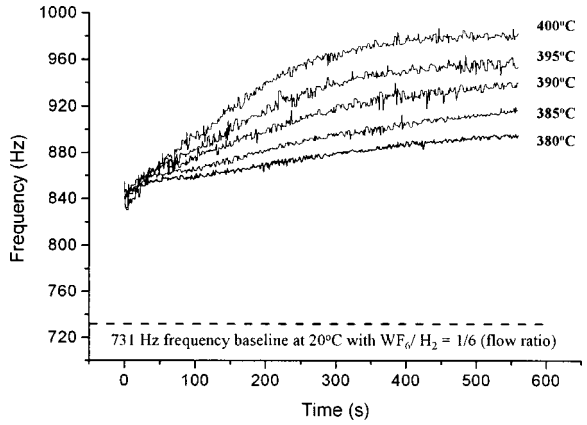

FIG. 6. Resonant frequency response overlaid over five runs at different temperatures. The decrease of the WF_6 depletion at lower temperature is sufficient to generate a noticeable variation of the average molecular weight of the gas mixture and therefore of the monitored resonant frequency.

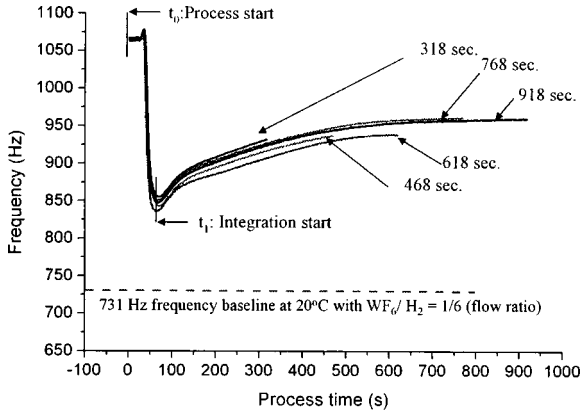

FIG. 8. Resonant frequencies vs process times are overlaid for five processes at 10 Torr and 390 °C during the exact time when the WF_6 and H_2 gases are flowed into the chamber. Process times were varied in the following order: 618, 468, 768, 318, and 918 s.

linear correlation could not be established over the 60 °C temperature range, which corresponds to a film thickness ranging from 400 to 1800 nm. Instead, two local regions were distinguished as a function of the temperature range, each of which could be fit with a first-order relation, and from each we obtained a similar metrology error of 0.8%. Such nonlinearity was also observed with other *in situ* sensing methods (e.g., mass spectrometry), which suggests that the amount of deposited tungsten on the wafer actually did not vary linearly over the full 60 °C temperature range. The lower slope in the high temperature regime as well as visual observations of the process chamber suggest that the tungsten deposition occurred more rapidly on other surfaces of the reactor (such as the showerhead) once a certain temperature was reached. However, varying the growth rate by a factor of 4 as a result of a wafer temperature drift clearly corresponds to a unrealistic case for an operational manufacturing tool (unless of a major tool failure), and it therefore appears correct to consider only linear models within a limited temperature regime.

D. Process time as a potential process control variable

A final set of experiments was carried out where the deposition times were varied from 5 to 15 min while other process variables were kept constant. Ten wafers were processed at 390 °C and 10 Torr for five different deposition times in the following order: 618, 468, 768, 318, and 918 s. In Fig. 8, the frequency monitored for 5 of these runs is plotted as a function of the deposition time. Despite the fixed process conditions, the resonant frequency appears to increase over all runs but the last one (918 s). This apparent decrease in the overall depletion of the WF_6 precursor from run-to-run is consistent with the drift observed during the first set of experiments under fixed conditions (see Fig. 5).

Figure 9 shows the correlation between the W film weight and the integration of the frequency signal. In this case the best fit was obtained with a second order mathematical expression with a regression coefficient $R^2=0.998$. The average error for the film thickness metrology based on this polynomial fit is equal to 1.0%.

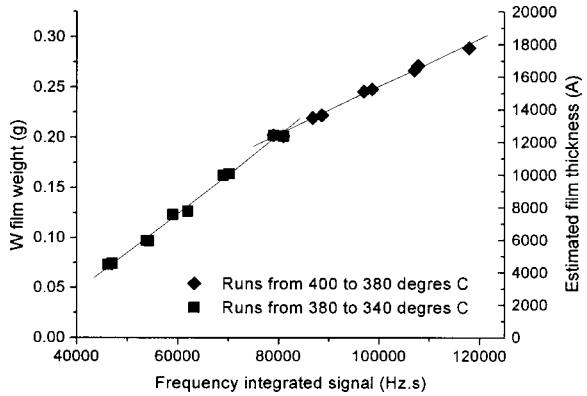

FIG. 7. *In situ* film thickness metrology obtained over 18 wafers processed for 618 s at 10 Torr. The temperature was varied from 400 to 340 °C resulting in variation of the growth rate by a factor of 4. A 0.8% metrology error was established over two local linear fits shown on the graph.

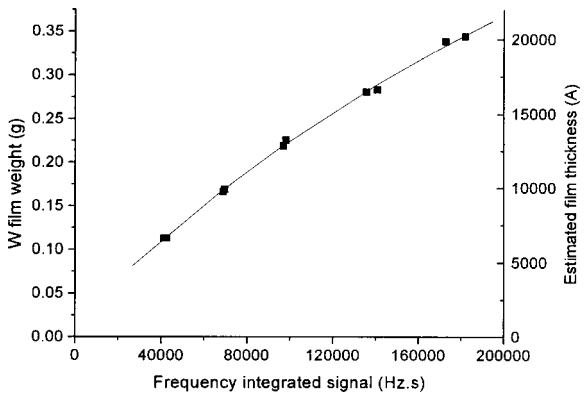

FIG. 9. W film weigh vs sensor based integrated measurements for ten wafers processed at 10 Torr and 390 °C for deposition times varying from 318 to 918 s. A 1.0% film thickness metrology was established based on the shown second order polynomial fit.

V. DISCUSSION

As we had shown in our previous publication,[31] these results confirm that downstream gas phase acoustic measurements can provide a viable means to real-time, *in situ* sensor-based metrology in a multicomponent CVD process. In this case, a correlation could be readily expressed between the integrated resonant frequency and the deposited film thickness, using either a linear or non-linear regression analysis to establish a sensor model with an accuracy better than 1%. This was achieved in a 10 Torr W CVD process, as illustrated both by using fixed process conditions and by intentionally introducing experimental process drifts. The significant improvement in metrology accuracy compared to our previous published data results primarily from the high depletion rate (up to 30%) of the WF_6 precursor which occurs in this elevated pressure regime. Because of the high mass ratio between WF_6 and H_2, the high depletion rate produced variations of the mass-dependent resonant frequency up to 200 Hz, or nearly two orders of magnitude above the noise level. This is a significant improvement over the previously established metrology at 0.5 Torr, where low depletion levels of 5% or less resulted in a metrology error of 6%. Clearly, higher depletion or reaction rates produce better metrology that is based on reactant depletion and/or product generation.

Even though the current work has not been extended to real-time control applications, the mechanism for doing so has been described in details in our prior group's publication using mass spectrometry as the sensor-based metrology.[22] In that work, a similar correlation between the integrated mass-spectrometer signal and the deposited film thickness had been established with an error of 1%–1.5%, which in turn enabled a demonstration of real-time end-point control of film thickness to a comparable accuracy. We therefore believe that the present results provide a very good prognosis for the use of acoustic sensing as a real-time thickness metrology and control strategy.

A. Importance of signal time integration

End-point control of the deposited film thickness can be most easily achieved by varying the process time to control the film thickness: the process is continued until a target for the sensor-based signal is reached, with the target determined from a metrology plot such as shown in Figs. 5 or 7. In this simple control algorithm, the process time is defined as the primary control variable while the sensor-based signal represents the secondary control variable. This implies that the sensor-based signal must be integrated in order to provide a cumulative variable reflective of the deposition occurring across the entire process cycle.

The choice of the frequency baseline used for the integration must be determined carefully. Contrary to other chemical sensors (e.g., mass spectrometry, which monitors specific partial pressures), a zero sensor signal has no physical meaning and is not correlated to a specific gas composition. It consequently does not make sense to choose the zero as a base line for the measurements and the integration. Instead, as shown in Fig. 4, the integration was calculated from the baseline at 731 Hz that corresponds to the frequency of a H_2/WF_6 gas mixture for a 6/1 flow ratio at room temperature. Deviation of the sensor frequency from this base line can be related to the consumption of the precursor and indirectly to deposition of W on the wafer. It must be noted that the frequency value for this base line can be determined easily in two ways, either by experimental measurement prior to the process runs for the given process gas flow ratio, or by calculation using Eq. (1). Therefore, determining the base line should not degrade process cycle time, which is critical in manufacturing applications.

To achieve good metrology, it is also essential to determine accurately when to start and stop the integration of the sensor signal which generates the metrology metric. In this study, we have chosen to do the postprocess integration from the time when the N_2 was flushed from the cell by the process gases (see Fig. 8), so that the monitored frequency corresponds to the evolution of the composition in the reactor in a physically sensible way. For advanced process control, the procedure can be simplified by automatically starting the integration from the time when the H_2 and WF_6 mass flow controllers are opened. Since the sampling system response time is consistent from wafer to wafer, the extra integrated area remains a constant and does not affect the metrology accuracy. It must be noted that the sensor response time at the start of the process could be improved in several ways, including the use of a more compact sampling system with reduced tubing length, and more compact pressure and flow gauges. Increasing the gas throughput into the acoustic cell is also an alternative, though it might require a sampling location farther downstream to the process to avoid disturbing the flow distribution in the chamber. Reducing the pressure in the sampling system by a given factor will reduce the response time by the same amount but decreasing the pressure down to its operational limit at 50 Torr will increase the noise/signal ratio and might affect the metrology.

B. Nonlinearities in sensor-based metrology

Contrary to other *in situ* chemical sensors that we have used for film thickness metrology (e.g., mass spectrometer or FTIR optical sensors), the response of the acoustic sensor to composition variations is inherently nonlinear. This can be seen from Eq. (1), where the resonant frequency varies as an inverse function of the square root of the average molecular weight of the gas mixture. The nonlinearity is also clearly shown by the simulation results shown in Fig. 10, which illustrates the variation of the resonant frequency while the WF_6 depletion rate varies from 0% to 100%, assuming an initial gas mixture corresponding to the one used in the process (e.g., 10 sccm WF_6, 60 sccm H_2).

The experimental data points in Fig. 10 were established from the 18 runs where the process temperature was varied from 400 to 340 °C. The resonant frequencies were determined at the end of the process, when the process conditions tend to be steady (see Fig. 4), while the depletion rates were estimated from the weight of tungsten deposited on the wa-

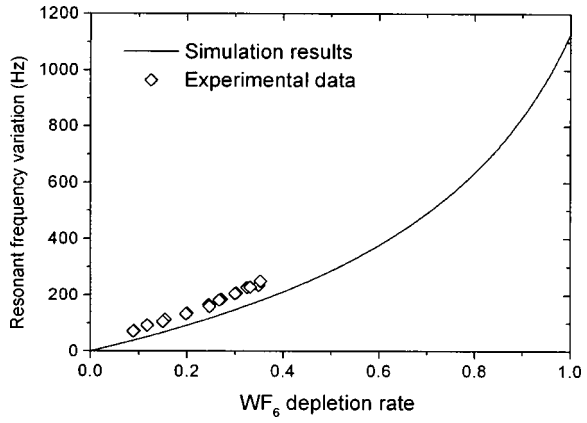

FIG. 10. Variation of the resonant frequency vs WF_6 depletion rate. The simulation results show the nonlinearity of the acoustic sensor response as the WF_6 depletion rate during the CVD process increases from 0% to 100%. Experimental results were obtained from 18 runs at 400–340 °C, the depletion being estimated from the weight of the deposited W film on the wafer. The offset between simulation and experimental data is due to the deposition of W on other surfaces than the wafer, which was not accounted for to estimate the experimental value of the depletion.

fer. Such an estimate of the depletion rate is in principle incorrect since it would assume that WF_6 only reacts on the wafer and not on other surfaces of the reactor.

The difference between the simulation and experimental data is probably a good indicator of the fraction of WF_6 that is effectively deposited on the wafer, as opposed to that deposited elsewhere in the reactor. For example, for the first run at 400 °C the depletion of WF_6 generated a resonant frequency variation of 250 Hz from the base line at 731 Hz, this base line corresponding to a 0% depletion condition (room temperature condition). Based on the film weight, the corresponding depletion rate was 35.3% while the simulation results show that a 45.4% depletion would be required to generate a similar variation of the resonant frequency, i.e., a 10% difference that can be attributed to the amount of WF_6 deposited on the walls and reactor showerhead. The ability to anticipate accurately the response of the acoustic sensor for a given set of conditions in the reactor (see Fig. 2) may thus be useful to quantify the amount of depletion occurring on other surfaces than the wafer.

The nonlinearity of the sensor is clearly displayed in Figs. 7 and 9. Of course it is desirable and more convenient to have linear rather than nonlinear sensor response, but for metrology and process control applications it is by no means required. A useful sensor-based metrology is achieved if: (1) the relation between the sensor output and the metric to be controlled is well defined (e.g., of order 1% for the manufacturing applications we seek), and (2) this relation is robust with respect to the range of process drifts in the application.

As seen in Figs. 7 and 9, the nonlinearity in sensor response can be fit to achieve a sensor model either by a nonlinear relationship or by a set of linear fits over a more limited range of process parameters. In these data, the nonlinearities are apparent because the results cover a wide range of process conditions (e.g., temperature variations of 40 °C resulting in a variation of the growth rate by a factor of 4 or process times varying from 5 to 15 min), and for some application (particularly in development) the sensor capability to provide metrology over a broad range is valuable. For advanced process control applications in manufacturing, however, one would expect a need for quantitative sensor accuracy only over a small range of process parameters, specifically to sense minor drifts in the process and enable compensation for them in real-time or run-to-run process control. In this case, the accuracy of the metrology is even higher, and linear models for sensor response are adequate.

VI. CONCLUSION

An acoustic sensor was implemented downstream to a W CVD chamber where processes were carried at 10 Torr using WF_6 and H_2 gas mixtures. A real-time, *in situ* film thickness metrology with an error of 1.0% or less was successfully established over 30 runs carried out either under fixed process conditions or while varying the process temperatures or deposition times to simulate process and equipment variability. This metrology accuracy, consistent with requirements to deliver value for manufacturing processes, was achieved when significant reactant depletion rates are present, as typically encountered in manufacturing. To establish the metrology, the sensor-based data were integrated over the process time to provide a cumulative thickness metric during each wafer run. These results present a very good prognosis for exploiting *in situ* chemical sensors, and in particular acoustic sensors, as the basis for real-time thickness metrology and corresponding real-time advanced process control.

[1]S. W. Butler, J. Hosch, A. C. Diebold, and B. V. Eck, Future Fab Int. **1**, 315 (1997).
[2]M. Miller and C. Bode, Future Fab Int. **12** (2002).
[3]*National Technology Roadmap for Semicondutors*, 2001.
[4]J. Pei, F. L. Degertekin, B. T. Khuri-Yakub, and K. C. Saraswat, Appl. Phys. Lett. **66**, 2177 (1995).
[5]W. Zhang, M. Ritcher, P. Solomon, Y. Kostoulas, W. Aarts, and A. Waldhauer, Solid State Technol. (1998).
[6]W. J. DeSisto, E. J. Cukauskas, B. J. Rappoli, J. C. Culbertson, and J. H. Claassen, J. Chem. Vap. Deposition **5**, 233 (1999).
[7]W. J. DeSisto and B. J. Rappoli, J. Cryst. Growth **170**, 242 (1997).
[8]W. J. DeSisto and B. J. Rappoli, J. Cryst. Growth **191**, 290 (1998).
[9]K. Hanaoka, H. Ohnishi, and K. Tachibana, Jpn. J. Appl. Phys., Part 1 **32**, 4774 (1993).
[10]J. A. O'Neill, M. L. Passow, and T. J. Cotler, J. Vac. Sci. Technol. A **12**, 839 (1994).
[11]K. Hanaoka, H. Ohnishi, and K. Tachibana, Jpn. J. Appl. Phys., Part 1 **34**, 2430 (1995).
[12]K. Hanaoka, K. Tachibana, and H. Ohnishi, Thin Solid Films **262**, 209 (1995).
[13]S. Salim, C. A. Wang, R. D. Driver, and K. F. Jensen, J. Cryst. Growth **169**, 443 (1996).
[14]A. Y. Kovalgin, F. Chabert-Rocabois, M. L. Hitchman, S. H. Shamlian, and S. E. Alexandrov, J. Phys. IV **5**, 357 (1995).
[15]R. W. Cheek, J. A. Kelber, J. G. Fleming, R. S. Blewer, and R. D. Lujan, J. Electrochem. Soc. **140**, 3588 (1993).
[16]L. L. Tedder, G. W. Rubloff, I. Shareef, M. Anderle, D. H. Kim, and G. N. Parsons, J. Vac. Sci. Technol. B **13**, 1924 (1995).
[17]L. L. Tedder, G. W. Rubloff, B. F. Cohaghan, and G. N. Parsons, J. Vac. Sci. Technol. A **14**, 267 (1996).
[18]L. Guangquan, L. L. Tedder, and G. W. Rubloff, J. Vac. Sci. Technol. B **17**, 1417 (1999).
[19]T. Gougousi, Y. Xu, J. N. Kidder, G. W. Rubloff, and C. R. Tilford, J. Vac. Sci. Technol. B **18**, 1352 (2000).

[20]T. Gougousi, R. Sreenivasan, Y. Xu, L. Henn-Lecordier, G. W. Rubloff, J. N. Kidder, Jr., and E. Zafiriou, AIP Conf. Proc. 249 (2001).
[21]R. Sreenivasan, T. Gougousi, X. Yiheng, J. Kidder, E. Zafiriou, and G. W. Rubloff, J. Vac. Sci. Technol. B **19**, 1931 (2001).
[22]Y. Xu, T. Gougousi, L. Henn-Lecordier, Y. Liu, C. Soon, and G. W. Rubloff, J. Vac. Sci. Technol. B **26**, 2351 (2002).
[23]B. R. Butler and J. P. Stagg, J. Cryst. Growth **94**, 481 (1989).
[24]A. Wajid, C. Gogol, C. Hurd, M. Hetzel, A. Spina, R. Lum, M. McDonald, and R. J. Capik, J. Cryst. Growth **170**, 237 (1997).
[25]J. P. Stagg, J. Christer, E. J. Thrush, and J. Crawley, J. Cryst. Growth **120**, 98 (1998).
[26]S. Yamamoto, K. Nagata, S. Sugai, A. Sengoku, Y. Matsukawa, T. Hattori, and S. Oda, Jpn. J. Appl. Phys., Part 1 **38**, 4727 (1999).
[27]S. Yamamoto, S. Sugai, and S. Oda, J. Phys. IV **9**, 1013 (1999).
[28]M. G. Flynn, R. Smith, P. Abraham, and S. DenBaars, IEEE Trans. Control Syst. Technol. **9**, 728 (2001).
[29]A. Wajid, Rev. Sci. Instrum. **71**, 3461 (2000).
[30]A. Wajid, Rev. Sci. Instrum. **67**, 1961 (1996).
[31]L. Henn-Lecordier, J. N. Kidder, G. W. Rubloff, C. A. Gogol, and A. Wajid, J. Vac. Sci. Technol. A **19**, 621 (2001).
[32]L. Guangquan, M. Bora, L. L. Tedder, and G. W. Rubloff, IEEE Trans. Semicond. Manuf. **11**, 63 (1998).